Structure–fluorescence correlations in a single tryptophan mutant of carp parvalbumin: Solution structure, backbone and side-chain dynamics

ARTICLE *in* JOURNAL OF MOLECULAR BIOLOGY · APRIL 2000

Impact Factor: 4.33 · DOI: 10.1006/jmbi.2000.3549 · Source: PubMed

6 AUTHORS, INCLUDING:

Nenad Juranic
Mayo Foundation for Medical Education and …
199 PUBLICATIONS **2,340** CITATIONS
SEE PROFILE

James D Potter
University of Miami Miller School of Medicine
202 PUBLICATIONS **7,798** CITATIONS
SEE PROFILE

doi:10.1006/jmbi.2000.3549 available online at http://www.idealibrary.com on IDEAL® J. Mol. Biol. (2000) 297, 147–163

JMB

Structure-Fluorescence Correlations in a Single Tryptophan Mutant of Carp Parvalbumin: Solution Structure, Backbone and Side-chain Dynamics

Martin C. Moncrieffe[1], Nenad Juranić[1], Marvin D. Kemple[2] James D. Potter[3], Slobodan Macura[1] and Franklyn G. Prendergast[1]*

[1]*Department of Biochemistry and Molecular Biology, Mayo Foundation, 200 First St. SW Rochester, MN 55905, USA*

[2]*Department of Physics, Indiana University Purdue University Indianapolis Indianapolis, IN 46202, USA*

[3]*Department of Molecular and Cellular Pharmacology University of Miami Sch. of Medicine, Miami FL 33101, USA*

Heterogeneous fluorescence intensity decays of tryptophan in proteins are often rationalized using a model which proposes that different rotameric states of the indole alanyl side-chain are responsible for the observed fluorescence lifetime heterogeneity. We present here the study of a mutant of carp parvalbumin bearing a single tryptophan residue at position 102 (F102W) whose fluorescence intensity decay is heterogeneous and assess the applicability of a rotamer model to describe the fluorescence decay data. We have determined the solution structure of F102W in the calcium ligated state using multi-dimensional nuclear magnetic resonance (NMR) and have used the minimum perturbation mapping technique to explore the possible existence of multiple conformations of the indole moiety of Trp102 of F102W and, for comparison, Trp48 of holo-azurin. The maps for parvalbumin suggest two potential conformations of the indole side-chain. The high energy barrier for rotational isomerization between these conformers implies that interwell rotation would occur on time-scales of milliseconds or greater and suggests a rotamer basis for the heterogeneous fluorescence. However, the absence of alternate Trp102 conformers in the NMR data (to within 3 % of the dominant species) suggests that the heterogeneous fluorescence of Trp102 may arise from mechanisms independent of rotameric states of the Trp side-chain. The map for holo-azurin has only one conformation, and suggests a rotamer model may not be required to explain its heterogeneous fluorescence intensity decay. The backbone and Trp102 side-chain dynamics at 30 °C of F102W has been characterized based on an analysis of ^{15}N NMR relaxation data which we have interpreted using the Lipari-Szabo formalism. High order parameter (S^2) values were obtained for both the helical and loop regions. Additionally, the S^2 values imply that the calcium binding CD and EF loops are not strictly equivalent. The S^2 value for the indole side-chain of Trp102 obtained from the fluorescence, NMR relaxation and minimum perturbation data are consistent with a Trp moiety whose motion is restricted.

Keywords: time-resolved fluorescence; NMR solution structure; dynamics; order parameters; minimum perturbation maps

**Corresponding author*

Introduction

Fluorescence spectroscopy is a popular tool for investigating protein structure and dynamics. Unavoidably, however, the fluorescence of a protein can report only indirectly; it is always necessary to infer the physicochemical behavior of the environment from the measured photophysical parameters predicated on the assumption that the photophysical responses to the environment are understood *a priori*. Inferences regarding the dynamics of the protein matrix and solvent are generally made from measurements of either the fluorescence intensity decays (lifetimes) or, from presumably direct determination of the rotational or librational

E-mail address of the corresponding author: prendergast@mayo.edu

0022-2836/00/010147–17 $35.00/0

motions of the fluorophore itself; such determinations being based on inferences drawn from fluorescence anisotropy decays and construction of plausible physical models.

The intensity decay of tryptophan (Trp) fluorescence in proteins and peptides, even those containing a single Trp moiety, is almost invariably heterogeneous requiring multi-exponential decay kinetics to describe the data (Beechem & Brand, 1985). A similar situation holds even for free Trp in aqueous solution at neutral pH (Szabo & Rayner, 1980) although the fluorescence of *N*-acetyl-tryptophanamide is generally agreed to be mono-exponential. A variety of models have been proposed in an attempt to rationalize the physical meaning of such heterogeneity, most of which, in one way or another, are based on the dynamics of the indole side-chain, hence by inference, the dynamics of the protein matrix. The rotamer model of Szabo & Rayner (1980) is fundamentally an extension of earlier work (Gauduchon & Wahl, 1978). The model proposes that different rotameric states of the alanyl side-chain of Trp are responsible for the observed heterogeneity, the proximity of the indole ring to the amino- and carboxy-functional groups being the principal determinants of the fluorescence lifetime. In contrast, the models of James *et al*. (1985) and Alcala *et al*. (1987) posit the existence of a quasi-continuous distribution of states which arises because the dynamics of the fluorophore allows it to sample multiple physical states each with a unique set of physicochemical interactions with the excited fluorophore giving rise to non-exponential decay. The width of the lifetime distribution is thought to reflect the number of unique microenvironments (conformational substates) sampled by the fluorophore and the rate of interconversions among these substates during the fluorescence lifetime. A third model that attempts to rationalize the fluorescence intensity decay of Trp is that of Bajzer & Prendergast (1993) which builds on the earlier findings of Petrich *et al*. (1983). At its core is the notion that heterogeneous fluorescence intensity decays may be obtained without the need to invoke the existence of different unique conformational states, or side-chain motions of the fluorophore *per se* as the heterogeneity is thought to result from quenching of the excited state by a variety of mechanisms not dependent on dynamics, the most probable being electron transfer. van Gilst *et al*. (1994) have proposed a fourth model which, in essence, is similar to that of Bajzer and Prendergast but includes specifically back transfer of an electron to a transient radical indole cation.

All of the above models can provide credible explanations for the existence of heterogeneous Trp fluorescence intensity decays and, given the complexity of protein structure, there is at present no justification *a priori* for choosing a particular model to explain the data in the absence of a clear structural basis for doing so. Ultimately, the selection of a particular model should depend on the availability of corroborating experimental or computational data. Thus, before invoking the rotamer model, for example, evidence must be adduced supporting the existence of the aforementioned rotamers for the system in question. Such evidence has been provided in peptides from high resolution nuclear magnetic resonance (NMR) data (Ross *et al*., 1992). Identification of relevant rotameric states in proteins may be difficult given that such states will not be detected by either NMR or X-ray crystallographic techniques unless they are sufficiently long lived and significantly populated. However, if the three-dimensional structure of the protein is known, computer simulations can be used to probe the possible existence of rotamers and should, at least in principle, allow quantitative assessment of the applicability of a rotamer model to explain the fluorescence decay data.

For experimental studies, the model chosen is obviously key. The least ambiguous data are likely to arise from proteins bearing a single Trp residue and preferably devoid of tyrosine, whose fluorescence intensity decay is heterogeneous. The tertiary structure of the protein should be known and preferably, the physicochemical properties should allow for measurement of the dynamics by both fluorescence and NMR spectroscopy. We have chosen to study a mutant form of carp parvalbumin which meets these criteria. Parvalbumins ($M_r \approx 12{,}000$), of which there are two classes, α and β, are acidic proteins which are predominantly found in fast-twitch muscle, usually at milli-molar concentrations intra-cellularly. Although their function remains uncertain, it appears that α-parvalbumins such as that from carp, serve as cytosolic calcium buffers; the β-isoforms are known to have immunomodulating properties (Brewer *et al*., 1989). The X-ray crystal structure of carp parvalbumin (Kretsinger *et al*., 1971; Moews & Kretsinger, 1975; Swain *et al*., 1989) reveals a compact globular protein having six α-helices denoted A-F whose packing delineate a hydrophobic core. Parvalbumins have three helix-loop-helix or EF-hand motifs (Kretsinger & Nockolds, 1973) which are numbered 2, 3 and 4 because the latter two domains are almost congruent with those of the homologous proteins calmodulin and troponin C (Kawasaki & Kretsinger, 1994). Domains 3 and 4, which are capable of binding both calcium and magnesium ions (Kawasaki & Kretsinger, 1994) are located between the C-D and E-F helices, respectively. The second domain, which does not bind metal ions, forms a cap covering the hydrophobic surface of lobes 3 and 4. The parvalbumin mutant used in this work is designated F102W and has the phenylalanine residue at position 102 in the wild-type protein replaced by Trp. The introduced Trp residue is immediately after the last metal-ion coordinating residue in site 4 ($-z+1$ of the calcium binding loop) and is in the same location as the naturally occurring Trp residue in whiting (Joassin & Gerday, 1977) and cod parvalbumin (Hutnik *et al*., 1990b). Indeed, the wavelength of maximum

fluorescence emission of F102W is similar to that reported for these two proteins (Hutnik *et al.*, 1990a,b; Eftink &Wasylewski, 1989). Furthermore, the absence of tyrosine residues in carp parvalbumin allows the unambiguous assignment of the fluorescence signal to the Trp residue.

This study was motivated primarily by one issue, namely, whether we could identify rotameric states of Trp from which we could rationalize heterogeneous fluorescence lifetimes. The value of such rationalization lies in defining the factors within the protein matrix which influence Trp dynamics. The ultimate objective is to engender confidence in our ability to use fluorescence techniques for detecting and quantifying protein dynamics. We determined the solution structure of F102W using multi-dimensional NMR spectroscopy to enable inferences between the environment of the indole side-chain and its fluorescence properties to be made. We then assess the likelihood that a rotamer model can explain the fluorescence intensity decay and order parameters of the indole side-chain of the introduced Trp residue of the mutant parvalbumin. A comparison to Trp48 of azurin (of *Pseudomonas aeruginosa*) is also made. The probability of side-chain rotamers was obtained by using the minimum perturbation mapping technique (Shih *et al.*, 1985; Haydock, 1993) which allows calculation of the potential energy surface for the indole side-chain as a function of its χ_1 and χ_2 dihedral angles. Additionally, we have sought to determine if the reported difference in the value of the overall rotational correlation time determined by NMR and fluorescence spectroscopy (Palmer *et al.*, 1993; Kemple *et al.*, 1994, 1997; Yuan *et al.*, 1996) is applicable to this parvalbumin mutant.

Results

NMR spectra, assignment and description of the structure

Figure 1 shows a representative 2D ^{1}H-^{15}N HSQC spectrum of calcium-saturated F102W at 30 °C. In general, the spectra were of high quality. Consequently, almost complete side-chain assignments of the residues in the protein were possible (Table A of Supplementary Material).

The three-dimensional structure of calcium saturated F102W was determined from the NMR data using a simulated annealing protocol from a total of 1039 NMR derived restraints. The 30 structures comprising the final ensemble all satisfy the distance restraints noted earlier with no violations greater than 0.5 Å and no dihedral violations greater than 5°. Table 1 details the NMR constraints used to generate the three-dimensional structures as well as the r.m.s.ds and XPLOR energies obtained for the calculation of the ensemble structures. The structures exhibit good covalent geometry as evidenced by the low r.m.s.ds from idealized values for bonds, improper and dihedral

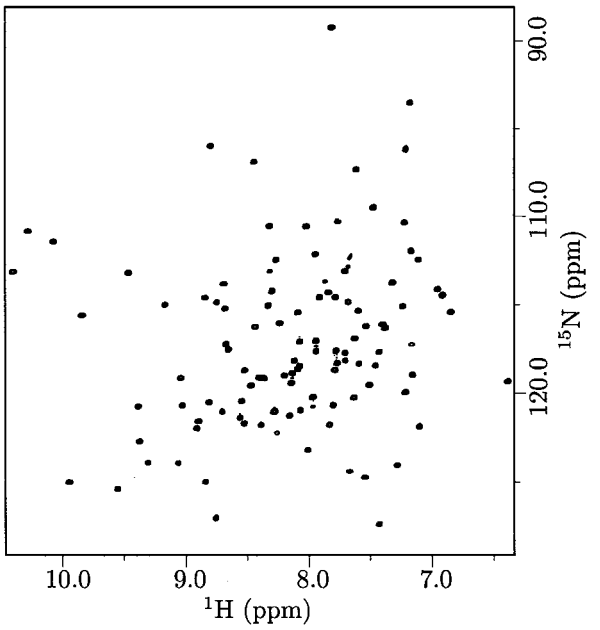

Figure 1. 2D ^{1}H-^{15}N HSQC spectrum of calcium-saturated F102W at 30 °C showing the amide proton-amide nitrogen correlations.

angles (Table 1). Figure 2 shows a Ramachandran plot of the ϕ and ψ angles for the 30 ensemble NMR structures as well as the computed average structure. For the average structure, all residues with the exception of Asp94 fall in the allowed regions of ϕ-ψ space with 77 % in the most favored region, ≈20 % in the additionally allowed regions and 2 % in the generously allowed region of the Ramachandran map. Of the 3240 residues in the 30 structures, only two residues, Ala21 and Asp53 have ϕ-ψ angles outside the allowed regions. The observed distribution of these angles is another indication of the quality of the obtained structures. Figure 3 shows the superposition of the 30 NMR structures onto the average structure. The backbone pairwise r.m.s.d. for the ensemble is 0.98(±0.22) Å for protons and 1.58(±0.22) Å for heavy atoms. Consequently, the structures of the backbone and core regions of the protein are well defined.

The structure of F102W obtained from the NMR data is shown schematically in Figure 4. There are six α-helices, A through F, as was observed in the X-ray crystal structure (Moews & Kretsinger, 1975) with the two calcium binding loops between the CD and EF helices. The α-helices are well defined superimposing with individual r.m.s.ds of 0.17(±0.08) Å (A), 0.10(±0.06) Å (B), 0.42(±0.27) Å (C), 0.31(±0.15) Å (D), 0.46(±0.17) Å (E) and 0.30(±0.09) Å (F) on the average structure. The inter-helical angle between helix C and D which

Table 1. Statistics of the conformational energies and r.m.s.d. for the ensemble of structures of parvalbumin F102W

Distance restraints	
Total	959
Short-range (intraresidue)	529
Sequential ($\|i-j\|=1$)	202
Medium-range ($2 \leqslant \|i-j\| \leqslant 4$)	115
Long-range ($\|i-j\| \geqslant 4$)	113
Dihedral restraints	80 ϕ
RMS deviations from idealized values	
Bonds (Å)	0.003 ± 0.000
Angles (deg.)	0.59 ± 0.01
Impropers (deg.)	0.47 ± 0.01
NOE (Å)	0.05 ± 0.00
Dihedrals (deg.)	0.49 ± 0.06
X-PLOR energies (kcal mol^{-1})	
E_{total}	358.2 ± 6.8
E_{bonds}	15.4 ± 0.6
E_{angles}	154.1 ± 2.6
E_{vdw}	51.6 ± 3.1
E_{NOE}	105.8 ± 5.7
E_{cdih}	2.9 ± 0.7
$E_{impropers}$	23.4 ± 1.1

comprise the first functional EF-hand is ≈109.7° while that between the E and F helix, the second EF-hand, is ≈92°. There is a break in the D helix at Leu65 which is consistent with the crystallographic data for the wild-type protein and F102W (Moews & Kretsinger, 1975; Cates *et al.*, 1999), and also with reports for pike parvalbumin (Alattia *et al.*, 1996).

The crystal structure of carp parvalbumin (Kretsinger *et al.*, 1971; Moews & Kretsinger, 1975; Swain *et al.*, 1989) and the NMR structure of the parvalbumin mutant F102W, are similar. The number of alpha helices, their length, as well as the disposition of these secondary structural elements are in good agreement with those observed crystallographically. The pairwise r.m.s.d. for the backbone atoms between the 1.6 Å resolution X-ray structure of carp parvalbumin and the average structure of F102W is approximately 1.5 Å while the value for non-hydrogen atoms is 2.2 Å. The C-D and E-F helices of these structures superimpose with r.m.s.ds of between 0.6 and 0.9 Å while the residues comprising the A and B helices have r.m.s.d.s of 1.4-2.0 Å. In the X-ray crystal structure of carp parvalbumin Phe102 and Val106 belong to the hydrophobic surface of the F-helix that interacts with Phe30 on the hydrophobic portion of helix B. With the introduction of the relatively bulky Trp side-chain there is the possibility that the hydrophobic core could be disrupted. The NMR and crystal (Cates *et al.*, 1999) structures of F102W indicate that the hydrophobic core is intact in the mutant protein. Trp102 is buried in the hydrophobic core and in addition to its proximity to Phe30, it is also close (⩽6 Å) to Phe47, Phe70, Phe85 and Phe66 (see Figure 4). Calculations of the solvent accessibility of Trp102 using both the Lee-Richards and Connoly algorithms suggest that this residue is buried and is ostensibly devoid of interactions with solvent. Additionally, the calculated Voronoi volume (Harpaz *et al.*, 1994; Gerstein *et al.*, 1995) of Trp102 is 225 Å^3, which is in good agreement with published values for a buried Trp residue (Harpaz *et al.*, 1994). In order to determine whether alternate conformations of the Trp side-chain exist, we have performed an HNC-type experiment (Grzesiek & Bax, 1992) which enables correlations between the H$^{\varepsilon 1}$, N$^{\varepsilon 1}$ and C$^{\delta 1}$ moieties of the indole ring of W102 to be made. The spectrum revealed a single such resonance suggesting, on the basis of the signal to noise ratio, that alternate conformations of W102 do not exist with a margin of error below 3 %.

NMR relaxation

Figure 5 shows examples of fits to a single-exponential function (see equation (1)) of the transverse- and longitudinal-relaxation data of the backbone amides and the N$^{\varepsilon 1}$H of W102. Figure 6 shows the relaxation parameters R_1, R_2 and $\{^1H\}^{15}N$ NOE obtained on ^{15}N-labelled protein at 500 MHz and the calculated R_{ex} and order parameters (S^2). ^{15}N relaxation data were obtained for 96 (500 MHz) and 97 (600 MHz) of the 108 residues. In fitting the relaxation data, an effective correlation time for internal motion, τ_e, was not required. However, the value of this parameter for the N$^{\varepsilon 1}$H vector of Trp102 was 0(±15) ps. For most residues the value of the exchange parameter, R_{ex}, was less than 1.5 s^{-1}. The correlation time representing the overall rotational motion of the molecule, τ_m, at 30 °C calculated from the R_1, R_2 and NOE data measured at 500 MHz is 4.76(±0.05) ns while that obtained from a combined analysis of the R_1 and NOE data at 500 MHz and 600 MHz is 4.63(±0.07) ns. These τ_m values are considerably shorter than the 8 ns value reported for the homologous rat α- and pike parvalbumin in the calcium-saturated state at 32 °C (Alattia *et al.*, 1996; Baldellon *et al.*, 1998). There are variations in the magnitude of the relaxation parameters throughout the sequence of the protein. Table 2 gives the average order parameters, $\langle S^2 \rangle$, for the helical and loop regions. Given that an order parameter of 1 represents an N-H vector that is immobile, the $\langle S^2 \rangle$ values obtained for the loop and helical regions of parvalbumin imply that these regions have limited mobility. The AB and BC loops appear to be the least immobile of the loop regions exhibiting lower $\langle S^2 \rangle$ values while the metal-binding CD loop appears to be more rigid in comparison to the second metal-binding EF loop. A closer examination of the S^2 values within the metal-binding loops reveals variations in the dynamic properties of the individual residues comprising the loop region. Table 3 shows the S^2 values for site III (CD-loop) and site IV (EF-loop). In general, the S^2 values for the backbone amide residues of the CD and EF-loops that are directly

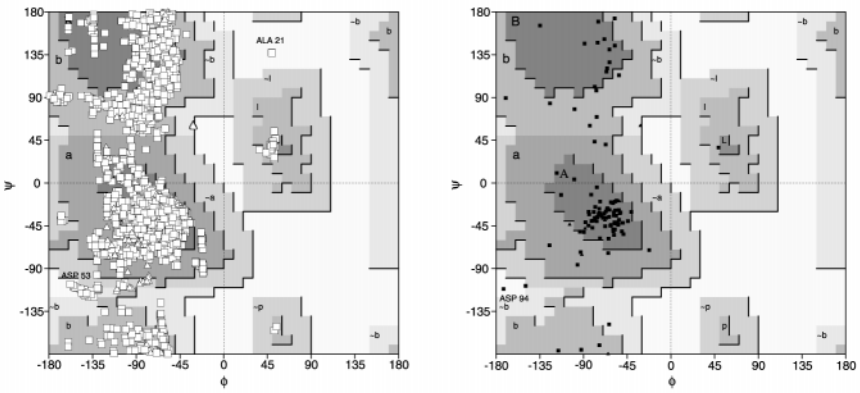

Figure 2. Ramachandran plot of the 30 ensemble NMR structures of F102W (left) and the average structure (right). For the 3240 residues comprising the ensemble structure, 74 % had ϕ-ψ distributions in the most favored regions (A, B, L), 23 % were in the additionally allowed regions (a, b, l, p) and 2.6 % in the generously allowed regions (~a, ~b, ~l, ~p). Only two residues, Ala21 and Asp53, had ϕ-ψ distributions in the disallowed regions. For the average structure, the corresponding ϕ-ψ distributions were 77 %, 20 %, 2 % with one residue, Asp94 in the disallowed region. Glycine residues are represented by triangles while all other residues are represented by squares. The plots were generated by the program PROCHECK-NMR (Laskowski *et al.*, 1996).

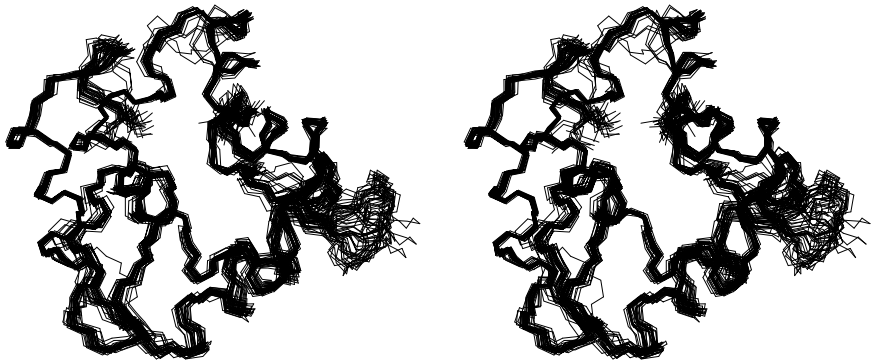

Figure 3. Cross-eye stereo image showing the backbone superposition of the 30 XPLOR generated structures for parvalbumin mutant F102W. The disordered region (lower right) occurs in the loop between the E and F helices.

involved in metal ion coordination are similar. However, this is not always so for the non-metal ion coordinating residues in the loops. The R_1, R_2 and NOE values for the $N^{\varepsilon 1}$-H vector of the indole side-chain of W102 are 2.23(±0.04) s^{-1}, 7.18(±0.12) s^{-1} and 0.76(±0.01), respectively and from these data the S^2 value is 0.84(±0.02).

Fluorescence

We have used time-resolved fluorescence to obtain information about the excited state lifetimes and the rotational dynamics of Trp102. Figure 7 shows typical time-resolved decay data for F102W

Table 2. Average order parameters, $\langle S^2 \rangle$, and their standard deviations, for the loop and helical regions of F102W obtained from the ^{15}N NMR relaxation data

Helix	$\langle S^2 \rangle$	Loop	$\langle S^2 \rangle$
A	0.89 ± 0.04	AB	0.85 ± 0.03
B	0.90 ± 0.05	BC	0.85 ± 0.05
C	0.91 ± 0.04	CD	0.97 ± 0.05
D	0.92 ± 0.04	DE	0.88 ± 0.03
E	0.90 ± 0.02	EF	0.89 ± 0.07
F	0.88 ± 0.04		

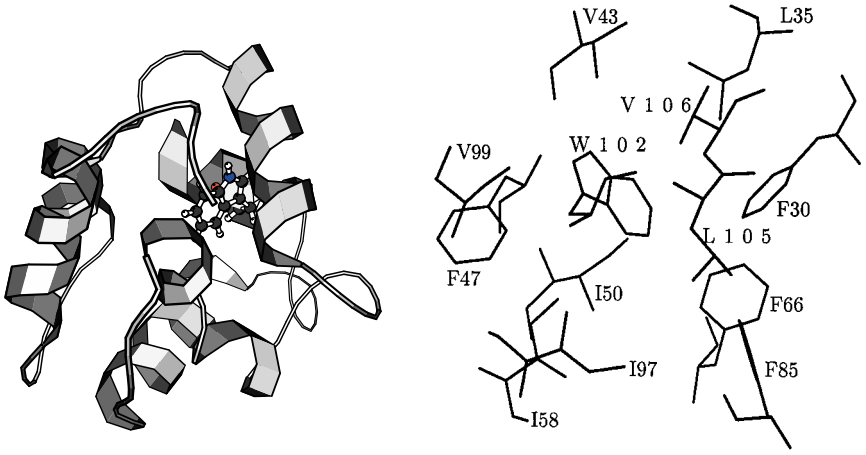

Figure 4. Elements of secondary structure of F102W and the location of Trp102 relative to these structural elements (left) and the hydrophobic residues that are within a 5 Å radius of Trp102 in the parvalbumin mutant F102W (right). The Figures were produced using MOLSCRIPT (Kraulis, 1991).

at 30 °C. Two lifetime components and two rotational correlation times describe the time-resolved fluorescence data as judged by several statistical criteria including *f*-tests applied to the Poisson deviances for models having different components and the randomness of the residuals (Catterall & Duddell, 1983). Table 4 shows the values recovered from an analysis of the time-resolved data of F102W at 20 and 30 °C. The long and short lifetime components (τ_1 and τ_2) are slightly shorter at 30 °C relative to their values at 20 °C. The fluorescence intensity at both temperatures is dominated by the long component which accounts for approximately 90 % of the total decay.

Table 3. Order parameters (S_a^2 and S_b^2) for residues in the metal-binding sites I and II of calcium-saturated F102W obtained from the NMR relaxation data

CD-loop			EF-loop		
Residue	S_a^2	S_b^2	Residue	S_a^2	S_b^2
D51$^{(X)}$	0.90(2)	0.92(2)	D90	0.91(2)	0.91(2)
Q52	0.97(6)	1.00(1)	S91	0.74(1)	0.74(1)
D53$^{(Y)}$	-	-	D92	0.92(1)	0.89(3)
K54	1.00(3)	1.00(1)	G93	0.83(1)	0.80(1)
S55$^{(Z)}$	1.00(4)	1.00(1)	D94	0.87(2)	0.88(3)
G56	0.93(3)	0.92(4)	G95	0.91(1)	0.92(1)
F57$^{(-Y)}$	1.00(2)	1.00(2)	K96	0.94(3)	0.94(3)
I58	0.87(2)	0.88(2)	I97	0.95(2)	0.95(3)
E59$^{(-X)}$	1.00(6)	1.00(1)	G98	0.94(2)	0.96(2)
E60	0.93(2)	0.94(2)	V99	0.90(2)	0.91(2)
D61	1.00(2)	1.00(1)	D100	0.83(2)	0.84(1)
E62$^{(-Z)}$	-	-	E101	0.83(1)	0.84(1)

S_a^2 was obtained from an analysis of the R_1 and NOE data measured at 500 MHz and 600 MHz while S_b^2 was obtained from an analysis of the R_1, R_2 and NOE data measured at 500 MHz only. The numbers in parenthesis are the uncertainties in least significant digit of the S^2 values and were obtained from 500 Monte Carlo simulations using the program MODELFREE 4.0 (Mandel *et al.*, 1995). *X*, *Y* and *Z* are the vertices to the calcium ligands.

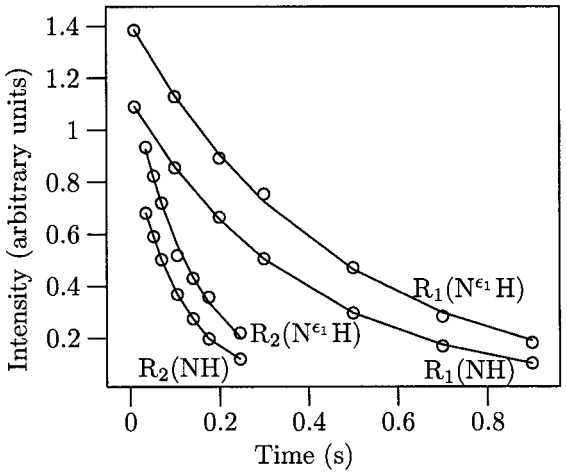

Figure 5. Examples of R_1 and R_2 decay curves for the backbone amide of W102 and the ε_{NH} of the indole side-chain of Trp102. The continuous lines are the best fits to single-exponential decays.

The time-resolved fluorescence anisotropy decay is dominated by the long rotational component which accounts for 83 % and 71 % at 20 and 30 °C, respectively. At 20 °C, the value of the long rotational component, ϕ_1, is 6.36(±0.20) ns and this decreases to 4.66(±0.12) ns at 30 °C. The ϕ_1 value is ascribed to the overall rotational motion while the short rotational correlation time (ϕ_2) is likely due to local motion of the indole moiety. If parvalbumin is assumed to be spherical, then its measured overall rotational correlation time should be close to the theoretically expected value. The rotational correlation time of a spherical molecule is given by $V_h\eta/kT$ where V_h is the hydrated specific volume, η is the solvent viscosity, k is Boltzmann's constant and T is the temperature in Kelvin. If V_h of parvalbumin is assumed to be 1 cm^3 g^{-1}, then the theoretical ratio of the overall rotational correlation time at 20 and 30 °C is 1.3. Given the ϕ_1 values determined by time-resolved fluorescence, the corresponding experimental ratio is 1.4. The low r_0 value implies that there are processes other than the overall rotational motion of F102W contributing to the depolarization of the fluorescence emission. Given that the rotational correlation time of free Trp in solution is approximately 40 ps, the recovered ϕ_2 value of 80 ps for Trp102 at 30 °C suggests that "local motions" of the indole side may be responsible, at least in part, for the observed depolarization. The amplitude of the fast motion associated with the short rotational correlation time can be assessed by calculating the fluorescence order parameter which is given by β_1/r_0 (Lipari & Szabo, 1982a) and for a specific model, $0.25(\cos^2\theta(1+\cos\theta)^2)$ where θ is the cone semi-angle within which the motion occurs (Kinosita *et al.*, 1977). Using the parameters recovered from the time-resolved fluorescence anisotropy decay of F102W at 30 °C, the order parameter associated with the rapid motion is 0.70 and $\theta = 27.5°$. The anisotropy at infinite time, r_∞, was 0 at both 20 and 30 °C.

Minimum perturbation mapping

We have used minimum perturbation mapping (Shih *et al.*, 1985; Haydock, 1993) to explore the possible side-chain conformations of Trp102 of F102W and Trp48 of azurin. Additionally, such maps allow estimates of the order parameters within, and isomerization between wells to be made (Haydock, 1993). Two minimum perturbation maps of F102W were generated. The first involved "mutating" Phe102 in the X-ray structure of wild-type carp parvalbumin to Trp while the second used the coordinates of the average NMR structure of F102W obtained in this work. The map for azurin was generated from the X-ray coordinates of Nar *et al.* (1991).

The maps for Trp102 both have two wells, one in the *trans*-perpendicular (tp) and the other in the *trans*-antiperpendicular (ta) orientation (see Figure 8(a) and (b)). For the map made from the average NMR coordinates, the tp well is stabilized

Table 4. Parameters recovered from an analysis of the time-resolved fluorescence anisotropy decay data of calcium saturated F102W at 20 and 30 °C

	ϕ_1 (ns)	ϕ_2 (ns)	β_1	β_2	r_0	χ^2
20°C	6.36 ± 0.20	0.16 ± 0.02	0.10 ± 0.01	0.02 ± 0.01	0.12 ± 0.01	1.3
30°C	4.66 ± 0.12	0.08 ± 0.01	0.10 ± 0.01	0.04 ± 0.01	0.14 ± 0.01	1.3
	τ_1 (ns)	τ_2 (ns)	α_1	α_2		
20°C	4.31 ± 0.01	1.12 ± 0.03	0.91 ± 0.01	0.09 ± 0.01		
30°C	4.12 ± 0.01	1.29 ± 0.03	0.89 ± 0.01	0.11 ± 0.01		

The two rotational correlation times ϕ_1 and ϕ_2 and their corresponding amplitudes, β_1 and β_2 as well as the two lifetime components τ_1 and τ_2 and their normalized amplitudes α_1 and α_2 are shown. The uncertainties in the recovered parameters were obtained from 100 Monte-Carlo simulations. The protein concentration was 7 μM and the solution composition was as described in Materials and Methods.

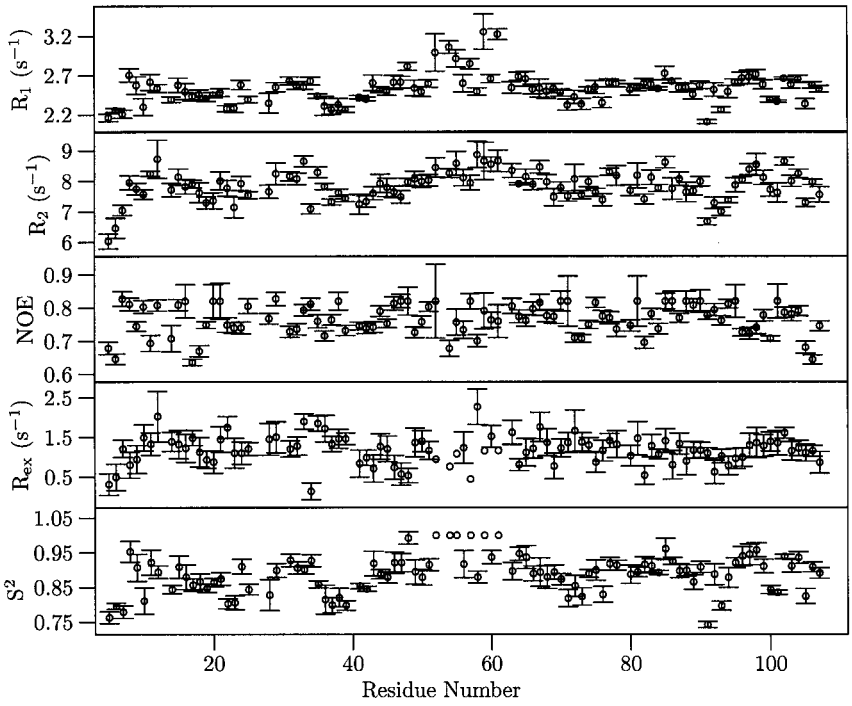

Figure 6. Relaxation rates (R_1, R_2), heteronuclear NOE, the generalized order parameter (S^2) and the conformational exchange parameter (R_{ex}) as a function of residue number for calcium saturated F102W. The error-bars in R_1 and R_2 are the standard errors obtained from fitting the data to equation (1) while those in R_{ex} and S^2 were obtained using the Monte Carlo procedure in the program MODELFREE 4.0.

by 1.3 kcal/mol relative to the ta well while in the map generated from the X-ray coordinates, the tp well is stabilized by 0.65 kcal/mol. The energy barrier between the wells is greater than 50 kcal/mol. The minimum perturbation map of Phe102 (Figure 8(c)) of wild-type parvalbumin also shows two potential conformations not radically dissimilar to those simulated for Trp102. We will later explore the possible significance of this result. Interestingly, the map for azurin (Figure 8(d)) has a single well in the *trans*-antiperpendicular orientation which suggests that there is only one rotamer possible for the indole side-chain of Trp48. The order parameters calculated for motion in the ta and tp wells for the ^1L_a and ^1L_b fluorescence transition dipole of Trp102 of parvalbumin F102W and the $C^{\delta 1}$-H and $C^{\varepsilon 1}$-H NMR probe dipole following the procedure first described by Szabo (1984) and subsequently by Haydock (1993) are 0.91-0.98.

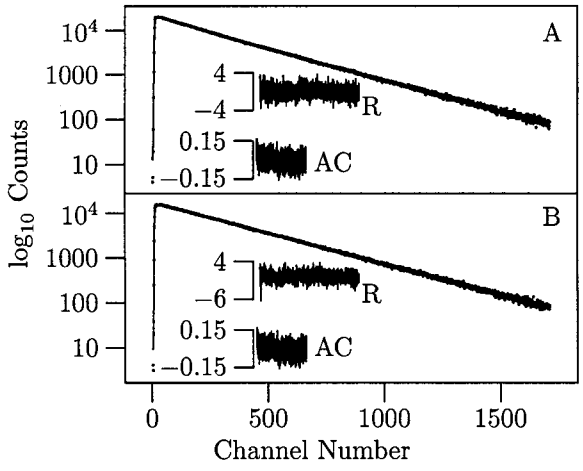

Figure 7. Data (···) and fits (—) of the (a) parallel and (b) perpendicular polarized components of the intensity decay of calcium saturated F102W at 30 °C (left). The inserts are the residuals (R) and auto-correlation (AC). Each channel represents a ''time-point'' of approximately 13 ps. Protein concentration was 7 μM.

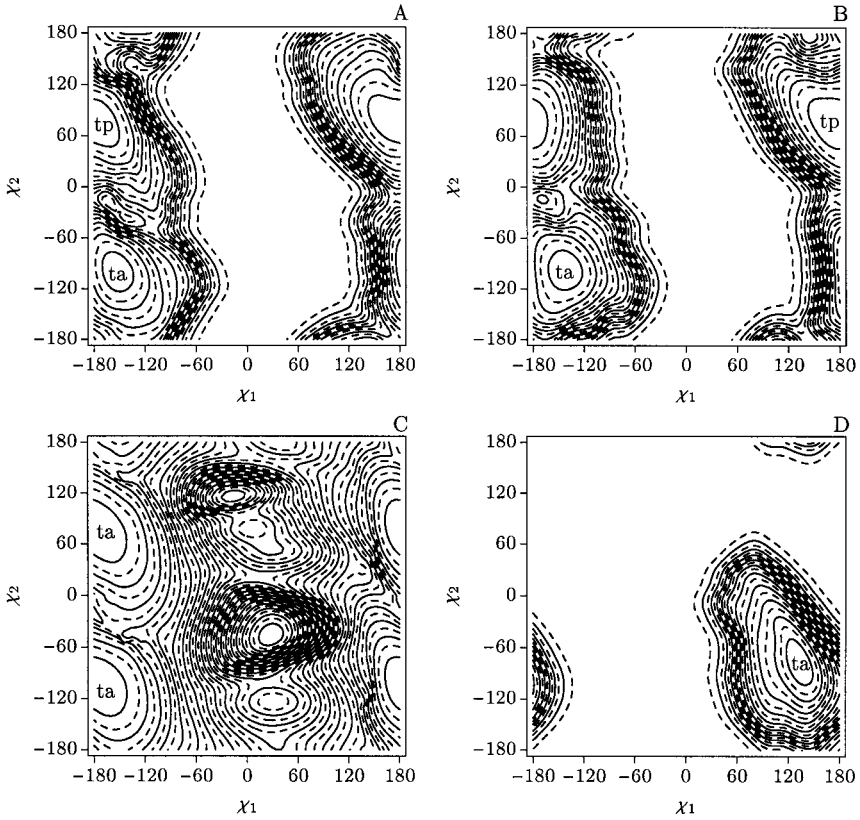

Figure 8. Minimum perturbation maps of Trp102 $\chi_1 \times \chi_2$ isomerization in the F102W mutant of carp parvalbumin starting from the simulated X-ray (a) and the NMR coordinates (b). The maps for Trp102 have wells in the *trans*-perpendicular (tp) and *trans*-antiperpendicular (ta) orientation as does the map of Phe102 of wild-type carp parvalbumin (c). The map for Trp48 of azurin (of *Ps. Aeruginosa*) has one well in the ta orientation (d). The contour lines are approximately 5 kcal/mol apart.

Discussion

Tryptophan fluorescence is widely used to make inferences about the structure and dynamics of proteins. This is due in part to the sensitivity of the fluorescence technique and the relative ease with which fluorescence data can be acquired. However, despite recent advances in calculating the wavelength of fluorescence emission of Trp residues in proteins (Callis, 1997), the interpretation of fluorescence data remains largely qualitative because the manner in which the protein matrix influences the fluorescence lifetimes is still poorly understood. Thus, although heterogeneous fluorescence intensity decays have been observed in the majority of proteins containing a single Trp residue (Beechem & Brand, 1985) for example, a variety of physical models can be employed for interpretation of this heterogeneity (Szabo & Rayner, 1980; Alcala *et al.*, 1987; Bajzer & Prendergast, 1993; van Gilst *et al.*, 1994). As also noted earlier, a primary objective was to determine whether a rotamer model could explain the fluorescence properties of Trp102 in parvalbumin F102W. We have reasoned that at the current state of our understanding of Trp photophysics in proteins, knowledge of the tertiary structure of F102W parvalbumin was essential. While this work was in progress, the crystal structures of this and other Trp102 bearing mutants of parvalbumin were reported (Cates *et al.*, 1999). Our tack was to determine the solution structure, primarily to evaluate whether the dynamics of the protein in solution, as opposed to the crystal, could in any way influence the inferences drawn from the time-resolved fluorescence data. We have also used ^{15}N-relaxation to measure directly the protein backbone and Trp side-chain dynamics.

The fluorescence emission of Trp is highly sensitive to the environment of the indole ring and emission maximum values range from 352 nm for a Trp moiety that is fully exposed to solvent (water) to 308 nm for Trp48 of azurin which is buried in a hydrophobic pocket (Hutnik & Szabo, 1989; Turoverov *et al.*, 1985). The fluorescence emission maximum of Trp102 of F102W is at 340 nm in the calcium-free state and at 320 nm (data not shown) in the calcium-saturated state. There are essentially two ways of rationalizing the 20 nm blue shift in the emission maximum in

going from the calcium-deplete to the calcium bound state. The traditional interpretation is that the environment of the indole moiety has changed from one that was solvent exposed to one devoid of solvent. While the absence of high resolution structural data for the metal-free state of parvalbumin makes it impossible to define precisely the character of the environment around the indole moiety of Trp102, the calculated static solvent accessible surface area of Trp102 in the calcium-saturated state suggests that the indole moiety is devoid of interaction with water. Callis (1997) has shown that large blue shifts of Trp fluorescence are possible if (i) a positive charge is close to the pyrrole ring or if (ii) a negative charge is close to the benzenoid portion of the indole ring. Examination of the structure of F102W suggests that the orientation of the calcium ion relative to Trp102 is such that the electric field does not project onto the long axis of the indole ring as would be required if the field from the bound calcium ion was responsible for the observed blue shift in the fluorescence emission. Consequently, the blue shift in the fluorescence emission that occurs in the calcium-saturated state relative to the metal-free state is likely the result of a calcium-induced conformational change that places Trp102 in a largely anhydrous environment.

The time-resolved fluorescence intensity and anisotropy decays of Trp102 are described by two lifetimes and two rotational correlation times. Applying the rotamer model we would infer the existence of two conformers (rotamers) of the indole side-chain to rationalize the fluorescence lifetime data. However, a fundamental question arises as to whether multiple Trp side-chain conformers are possible within the structural constraints imposed by the protein matrix packing, hence our use of the minimum perturbation mapping technique (Shih *et al*., 1985; Haydock, 1993). The central tenet of the minimum perturbation approach is that the difference in the structure of a stable mutant and the wild-type protein lies in the positions and flexibilities (dynamics) of the backbone and side-chain atoms which are neighbors of the mutant side-chain (Shih *et al*., 1985). Given that the Phe102 → Trp substitution in carp parvalbumin produces a stable mutant, the preceding implies that minimum perturbation maps calculated using coordinates derived from the three-dimensional solution structure of the mutant protein (obtained in this work) and that obtained from the coordinates of the wild-type protein in which the mutated residue has been introduced, should be similar. Figure 8(a)-(c) shows that maps obtained using coordinates derived from the NMR structure we determined and that obtained from the X-ray coordinates of the wild-type protein in which Phe102 was replaced by Trp or that calculated from the crystal structure are indeed very similar and suggest the possibility of two wells. This coincidence of findings is not surprising in view of the essential identity of the three structures but is especially important since the NMR structure is devoid of potential crystal lattice constraints.

For comparison, we have calculated maps for holo-azurin. The predicates for this comparison are the analogous locations of the Trp residues in the two proteins: in both cases the indole side-chain is buried in the protein matrix away from contact with water in distinctly hydrophobic environments; the Trp fluorescence spectra are substantially blue-shifted (azurin much more than parvalbumin) and the Voronoi volumes show that the packing densities of the environs of the Trp side-chain in both proteins is high; and the fluorescence lifetimes are heterogeneous in both proteins.

The map of holo-azurin (see Figure 8(d)) suggests a single rotamer making it difficult to justify a rotamer basis for the heterogeneous fluorescence decay of holo-azurin (Hutnik & Szabo, 1989; Hansen *et al*., 1990), a point noted earlier by Bajzer & Prendergast (1993) who suggested instead strictly photophysical processes involving, perhaps, electron transfer to the bound copper atom as the origin of the heterogeneity of lifetimes. This latter explanation is supported strongly by the mono-exponential decay of apo-azurin as it is known that removal of the copper atom causes no detectable conformational change in the protein. In the case of Trp102 of parvalbumin F102W, the situation is at first appearance different in that there are apparently two possible rotameric states of the indole side-chain. The similarity in the Voronoi volumes of Trp in parvalbumin F102W and azurin suggests moreover that the packing of the indole side-chain is not the sole determinant of the number of rotational isomers; that the dynamics of the surrounding protein matrix must influence the resulting side-chain conformations. On this basis therefore, one would predict that the neighboring residues of Trp48 of azurin are probably more conformationally constrained than those of parvalbumin F102W. Is there then any possible significance to the two wells in parvalbumin F102W suggested by the minimum perturbation maps? The high energetic barrier to conformational exchange between the wells suggested by the minimum perturbation maps implies that populating these isomeric states by inter-well rotation is implausible on the nanosecond timescale and would require timescales of milliseconds or greater. In our view the only way to significantly populate both is through ''trapping'' of a particular form as the protein folds, the form affording the lowest potential energy being the most probable. In other words, the sample would be conformationally inhomogeneous at least with regard to the Trp environment. However, given the signal to noise ratio in our NMR experiments, a second conformer of Trp102 is unlikely above 3% of the predominant conformation.

Analysis of the time-resolved fluorescence anisotropy decay of Trp102 yielded two rotational corre-

lation times at each of two temperatures, 20 and 30 °C. The ratio of the measured ϕ_1 values (correlation times for whole protein rotation) at 20 and 30 °C (1.4) is in good agreement with the theoretical ratio (1.3) calculated by use of the Stokes-Einstein formalism suggesting that the overall motion is isotropic. The ϕ_1 value obtained from the fluorescence anisotropy decay data at 30 °C (4.66 ns), is, within experimental error, identical to that obtained from the NMR relaxation measurements (4.63 and 4.76 ns) at the same temperature. This is in contrast to several reports in the literature where the results obtained by fluorescence and NMR are different (Palmer *et al*., 1993; Kemple *et al*., 1994, 1997) and also suggests that the overall rotational correlation time of 8 ns obtained for pike parvalbumin (Alattia *et al*., 1996; Baldellon *et al*., 1998) may have been due to protein aggregation.

The low pH used in the NMR experiments enabled observation of the $H^{\varepsilon 1}$ proton of Trp102. It is noteworthy that there was a single such resonance in keeping with the inference of a dominant conformation. The order parameter obtained for the $N^{\varepsilon 1}$-$H^{\varepsilon 1}$ vector from the NMR relaxation measurements should be comparable with that obtained from the decay of the fluorescence anisotropy. For this calculation, τ_m was fixed at the value obtained from the relaxation data of the backbone amides (4.76 ns) and the S^2 value was calculated using the $^{15}N^{\varepsilon 1}$ R_1 and NOE relaxation data assuming that the ^{15}N $\Delta\sigma$ is −126 ppm. Although we have not measured the ^{15}N $\Delta\sigma$ of the $N^{\varepsilon 1}$ nitrogen in F102W, the value used should allow a qualitative estimate of the order parameter for the indole moiety to be made. The calculated order parameter is $S^2_{-126\ \mathrm{ppm}} = 0.84(\pm 0.02)$, which is in good agreement with the value obtained from the time-resolved fluorescence anisotropy decay data. Thus, both the NMR and fluorescence data imply that the indole moiety of Trp102 is restricted.

The data above all support the notion of a rigidly held Trp side-chain solidly packed into the protein matrix devoid of contact with solvent. However, the question remains as to whether the backbone and side-chain dynamics of the protein as a whole might allow transient structural changes of sufficient magnitude to allow either ring rotation or water access. An examination of the generalized order parameters, taken as a whole set, corroborates the view of a physically very constrained protein. Recalling that Trp102 is adjacent to a calcium binding loop, we therefore paid particular attention to the apparent dynamics of the metal ligating regions. The NMR relaxation data for F102W suggest that while the helices and loop regions of parvalbumin exhibit high order parameters ($S^2 > 0.8$), the dynamics of the metal-ion binding loops are different. Published data suggest that the CD and EF sites of parvalbumin have equal affinities for calcium ($K_{D,Ca^{2+}} \approx 3 \times 10^9$ M) and for magnesium ($K_{D,Mg^{2+}} \approx 9 \times 10^4$ M) (Moeschler *et al*., 1980) and such data have been used to infer the equivalence of these sites. In contrast, Corson *et al*. (1983) while studying the binding of various lanthanides to carp (p*I* 4.25) parvalbumin found that one site had a nearly equal dissociation constant for La^{3+} and Lu^{3+} ($K_D = 4 \times 10^{-11}$ M) while the other showed a preference for La^{3+} ($K_{D,La^{3+}} = 2.0 \times 10^{-11}$ M; $K_{D,Lu^{3+}} = 3.6 \times 10^{-10}$ M). Thus, it is plausible that while the difference in the dynamics of the CD and EF loops are not the principal determinants of calcium or magnesium affinity in parvalbumin, this difference may be partially responsible for the trend observed with the lanthanides. A comparison of the S^2 data obtained for the backbone amides of F102W with similar data for other EF-hand proteins (Baldellon *et al*., 1998; Barbato *et al*., 1992; Akke *et al*., 1993; Gagne *et al*., 1998) reveals that the EF-hand, especially when metal ions are coordinated, is quite rigid with $S^2 > 0.8$. For calmodulin (Barbato *et al*., 1992) and rat α-parvalbumin (Baldellon *et al*., 1998) there is a tendency for the residue at relative position 2 of the second calcium-binding loop to have lower S^2 values relative to the other residues of the loop and this is observed with S-91 of F102W. The average S^2 values for the second calcium binding loop of F102W, calbindin D_{9k} and rat α-parvalbumin, in the calcium-saturated state are quite similar. However, the average S^2 for the CD loop of calcium-saturated F102W appears to be substantially higher than the corresponding loop of the other proteins and may point to a role for this region maintaining the stability of parvalbumin.

In summary, the NMR solution structure of parvalbumin F102W in the calcium-saturated state is similar to that of the wild-type protein determined by X-ray crystallography. The indole moiety is located in a hydrophobic core and is inaccessible to water. While the minimum perturbation maps suggest two non-interconverting (on the nanosecond timescale) conformations for the indole moiety of Trp102, the NMR data imply that the population of the minor conformer, if it exists, is $\leqslant 3\,\%$ of the more dominant species. In contrast, for Trp48 of holo-azurin it appears that there is only one possible rotamer of the indole side-chain and thus the heterogeneous fluorescence intensity decay of this protein results from processes other than rotational isomerization of the alanyl side-chain. The order parameters exhibited by the helices and loop regions of parvalbumin imply that the mobility of these regions is limited; the dynamics of the calcium binding CD and EF loops are different suggesting that these regions are not completely equivalent. In any event, main-chain dynamics do not provide a mechanism for more than one Trp rotamer. The overall rotational correlation time obtained from an analysis of the fluorescence and NMR relaxation data are, within experimental error, identical. Additionally, the calculated order parameter values for the indole side-chain of Trp102 obtained from the fluorescence, NMR and minimum perturbation maps are con-

sistent with an indole moiety whose internal motion is highly restricted. All of these results support the conclusion that for F102W, indole rotational isomerization does not occur on the fluorescence timescale and thus the heterogeneous fluorescence lifetimes of Trp102 apparently arise from quenching mechanisms independent of Trp rotameric states or the existence of two static distributions of protein conformations.

Materials and Methods

Protein preparation

The entire cDNA of carp parvalbumin was synthesized by the overlap fill-in method (Sambrook *et al.*, 1989) based on the published sequence (Coffee & Bradshaw, 1973). A Trp codon (TGG) was introduced by thermal cycling to replace Phe (TTC) at position 102. The mutated DNA was cloned into the *Nco*I-*Bam*HI cloning site of the pET3d expression plasmid. Mutations were verified by the standard dideoxy DNA sequencing method using the Sequenase II reagents (United States Biochemical, USA). Protein expression and purification were as described by Pauls & Berchthold (1993), with the following modifications. DNA in the pET3d plasmid was used to transform *Escherichia coli* strain BL-21 (DE3) cells and the expression checked on SDS PAGE gels. One milliliter of a log phase subculture was inoculated into one liter of Celtone-N (Martek Bioscience) for the preparation of ^{15}N enriched- or Celtone-CN for $^{13}C/^{15}N$-enriched protein.

Cultures were incubated in a dry rotary shaker to an A_{600} of 0.6-1.0 and IPTG was added to a final concentration of 0.4 mM. After four hours, the cells were pelleted at 4350 *g* for five minutes at 4 °C and resuspended in 20 mM imidazole (pH 8) containing 1 μM leupeptin and pepstatin and 10 μM PMSF at 30 ml/l of the original culture. The cell suspension was sonicated in an ice bath for six minutes in 60 seconds bursts with 90 seconds rests at level 8 with a Heat Systems (Famingdale, USA) sonicator. The sonicate was centrifuged for 30 minutes at 48,400 *g* and ammonium sulfate (to 70 % saturation) was added to the supernatant and the resulting solution stirred overnight at 4 °C. Contaminants along with a small amount of parvalbumin were pelleted at 48,400 *g* for 30 minutes and the supernatant dialyzed extensively against 40 mM imidazole. The dialyzed solution was loaded onto a DEAE Sephacel column equilibrated with the same solution and eluted with a 0-500 mM NaCl gradient. The purified PV fractions were subsequently pooled and dialyzed against one change of 50 volumes of 1 mM EDTA in 5 mM ammonium bicarbonate, and three changes of 50 volumes of 5 mM ammonium bicarbonate, then lyophilized and stored at −20 °C. The yield of purified protein obtained by this procedure was 80-120 mg/l. Samples for both NMR and fluorescence measurements were prepared by dissolving lyophilized protein in a medium composed of 0.1 M sodium citrate/citric acid (pH 5.6) containing approximately two equivalents of calcium. The final protein concentrations for the NMR and fluorescence measurements were 2-3 mM and 7-10 μM, respectively.

NMR spectroscopy

The following experiments were used to obtain sequential and side-chain assignments as well as NOE distance restraints and were acquired at 30 °C on a Bruker AMX 500 spectrometer equipped with a gradient probe (Bruker, USA): HCACO (Kay *et al.*, 1990), HCA(CO)N (Kay *et al.*, 1990), HN(CO)CA (Grzesiek & Bax, 1992), HNCA (Grzesiek & Bax, 1992), HNCO (Grzesiek & Bax, 1992), HNHA (Vuister & Bax, 1993), HCCH-COSY (Clore *et al.*, 1990), HCCH-TOCSY (Clore *et al.*, 1990), ^{15}N-TOCSY (Marion *et al.*, 1989), ^{13}C-TOCSY, ^{13}C-NOESY (Ikura *et al.*, 1990), ^{15}N-NOESY (Kay *et al.*, 1989a), ^{13}C-^{15}N-edited-NOESY (Zolnai *et al.*, 1995) and ^{1}H-^{1}H NOESY (Jeener *et al.*, 1979; Macura & Ernst, 1980). Backbone coupling constants, $^{3}J_{H^{N}H^{\alpha}}$ were measured using a ^{1}H-^{15}N-HMQC (Kay & Bax, 1990) experiment obtained on ^{15}N-labelled protein dissolved in 90% H_2O:10 %$^{2}H_2O$ and a 3D HNHA (Vuister & Bax, 1993) experiment. Table 5 gives the acquisition times in the time domains t_1, t_2 and t_3 where applicable, the final data block size of the processed matrices (D_1, D_2 and D_3) and the mixing times for the NOESY and TOCSY experiments. We have also performed an HNC-type experiment (Grzesiek & Bax, 1992) in which the ^{13}C carrier frequency was set to 117 ppm targeting the $C^{\delta 1}$ moiety of W102 and sufficient scans collected to achieve a signal to noise ratio of ≈1 %. For this experiment, the times in t_1, t_2 and t_3 were 5, 26 and 77 ms, respectively and the corresponding dimesions in the processed matrix were 1024, 512 and 64. ^{15}N-T_1, ^{15}N-T_2 and heteronuclear $\{^{1}H\}^{15}N$ NOE data were acquired at 30 °C using the pulse sequences developed by Kay *et al.* (1989b) on Bruker AMX 500 and DMX 600 (^{15}N-T_1 and $\{^{1}H\}^{15}N$ NOE) spectrometers. The relaxation delays for the T_1 experiments were 10, 100, 200, 300, 500, 700 and 900 ms while those for the T_2 experiments were 35, 53, 70, 106, 141, 176 and 246 ms. All NMR data sets were processed using the FELIX 95 software package (BIOSYM, USA). The T_1 and $\{^{1}H\}^{15}N$ NOE spectra were processed using a skewed sine-bell squared function (85 °) in both D_1 and D_2. For the other spectra, a Gaussian-to-Lorentzian apodization function was generally used in D_1 ($LB = -11$, $GB = 0.1$) and a skewed sine-bell squared function (85 °) in D_2 and D_3 where applicable. When linear-prediction was employed, the ''forward-backward'' method (Zhu & Bax, 1992) was used and the digital resolution in some spectra was increased using the program ZOOM (Zolnai *et al.*, 1996). Relaxation rates (R_i; $i = 1,2$) were obtained from fits of the peak intensities at different relaxation delays to a two-parameter function of the form:

$$I(t) = I_0 \exp(-R_i t) \tag{1}$$

where $I(t)$ is the peak intensity after a delay time t and I_0 is the intensity at $t = 0$. Fits of the peak intensities to a three-parameter function gave essentially the same results as the two-parameter fits. The relaxation rates (R_1 and R_2) and the NOE enhancement of the ^{15}N spin relaxed by the dipolar interaction with the attached proton and by the chemical shift anisotropy ($\Delta\sigma$) are given by (Abragam, 1961):

$$R_1 = \frac{d^2}{4}[J(\omega_H - \omega_N) + 3J(\omega_N) + 6J(\omega_H + \omega_N)] + c^2 J(\omega_N) \tag{2}$$

Table 5. Experiments used for the determination of the 3D NMR solution structure of F102W

Experiment	t_1	t_2	t_3	D_3	D_2	D_1	τ_{mix}
HCACO	13	19	93	256	256	128	n/a
HCA(CO)N	130	32	64	256	256	256	n/a
HN(CO)CA	32	9	85	256	256	256	n/a
HNCA	32	9	85	256	256	256	n/a
HNCO	32	18	85	256	256	128	n/a
HNHA	20	8	39	256	128	512	n/a
HCCH-COSY	19	8	30	256	256	256	n/a
HCCH-TOCSY	14	6	56	256	256	256	n/a
^{15}N-TOCSY	17	23	39	256	128	512	96
^{13}C-TOCSY	18	5	145	512	128	256	37
^{13}C-NOESY	18	7	28	256	256	256	150
^{15}N-NOESY	13	19	39	256	256	256	100
^{13}C-^{15}N-edited-NOESY	25	8	39	256	128	256	500
HN-HSQC	253	340	n/a	2048	4096	n/a	n/a
NOESY	73	73	n/a	2048	2048	n/a	200

The columns labelled t_1, t_2 and t_3 give the time (in milliseconds) spent in each time-domain. The mixing times (τ_{mix}) for the NOESY and TOCSY experiments are also given as are the dimensions of the processed matrices (D_1, D_2 and D_3).

$$R_2 = \frac{d^2}{8}[4J(0) + J(\omega_H - \omega_N) + 3J(\omega_N) + 6J(\omega_H) + 6J(\omega_H + \omega_N)] + \frac{c^2}{6}[4J(0) + 3J(\omega_N) + R_{ex} \quad (3)$$

and

$$NOE = 1 + \left(\frac{d^2}{4R_1}\right)\left(\frac{\gamma_N}{\gamma_H}\right)[6J(\omega_H + \omega_N) - J(\omega_H - \omega_N)] \quad (4)$$

in which $d = \mu_0\hbar\gamma_N\gamma_H/8\pi^2 r_{NH}^3$, $c = \omega_N\Delta\sigma/\sqrt{3}$, μ_0 is the permittivity of free space, $\hbar$ is Planck's constant, γ_H and γ_N are the gyromagnetic ratios of the ^{1}H and ^{15}N spin, r_{NH} is the N-H bond length ω_H and ω_N are the Larmor frequencies of the ^{1}H and ^{15}N nuclei and $\Delta\sigma$ is the ^{15}N $\Delta\sigma$. The relaxation data were analyzed using the Lipari-Szabo spectral density function (Lipari & Szabo, 1982a,b):

$$J(\omega) = \frac{2}{5}\left[\frac{S^2\tau_m}{1+\omega^2\tau_m^2} + \frac{(1-S^2)\tau}{1+\omega^2\tau^2}\right] \quad (5)$$

where τ_m is the overall rotational correlation time, S^2 is the generalized order parameter and τ_e is the effective correlation time for the internal motion of the N-H vector given by $\tau^{-1} = \tau_m^{-1} + \tau_e^{-1}$. For calculations which involved the use of transverse relaxation rates (R_2) an additional term, R_{ex}, was included to account for contributions from processes other than those from dipole-dipole (DD) and chemical shift anisotropy (CSA). The R_{ex} term modifies the calculated R_2 value as: $R_2 = R_{2(DD)} + R_{2(CSA)} + R_{ex}$. Calculations were performed using the program MODELFREE 4.0 (Mandel *et al.*, 1995) to obtain τ_m and S^2. We have taken the overall motion to be isotropic and have used *f*-tests to determine the optimum number of parameters required to adequately describe the relaxation data. A value of −160 ppm was used for the ^{15}N $\Delta\sigma$ for all backbone nitrogen atoms. Given the variation in the $\Delta\sigma$ as a function of the sequence for human ubiquitin (Fushman *et al.*, 1998), the value used here, is in effect, an average. For the N^{ε}_1 moiety of the indole ring a $\Delta\sigma$ value of −126 ppm was used based on the average value of the chemical shift tensor data of Hu *et al.* (1995).

Spectral assignment and structure calculation

Sequential assingments were obtained using standard procedures and utilized 3D NMR experiments (HCA(CO)N, HN(CO)CA, HCACO, HNCO, HNCA and HNHA) that enable connectivities through the protein backbone to be made. Side-chain assignments were obtained using HCCH-COSY, HCCH-TOCSY, ^{15}N-TOCSY and ^{13}C-TOCSY. The assignment of the aromatic ring protons of F102W was accomplished using a combination of 2D DQF-COSY and NOESY in ^2H_2O where connectivities through the ring were found on the DQF-COSY spectrum and the assignment to a particular residue was made from the observation of an NOE from the δ-protons to the β-protons.

The NOE cross-peaks obtained from the ^{13}C-NOESY, ^{15}N-NOESY, ^{13}C-^{15}N-edited-NOESY and the 2D ^{1}H-^{1}H NOESY experiments were calibrated taking the distance between two methylene protons as 1.8 Å. NOE intensities were classified as strong (1.8-2.7 Å), medium (1.8-3.5 Å) or weak (1.8-5.0 Å). Dihedral angle restraints were obtained from the three bond coupling constant ($^3J_{H^NH^\alpha}$) between the amide and alpha-proton. $^3J_{H^NH^\alpha}$ values were measured using 2D ^{1}H-^{15}N HMQC and 3D HNHA experiments and the allowed dihedral angle, ϕ, calculated using the Karplus equation (Pardi *et al.*, 1984). For helical regions ($^3J_{H^NH^\alpha} < 5$ Hz), the dihedral angle constraint $-80^\circ < \phi < -40^\circ$ is introduced while for $^3J_{H^NH^\alpha} > 8$ Hz the constraint is $-160^\circ < \phi < -80^\circ$.

The structure calculations were performed in two stages using modifications of the standard protocols in the program XPLOR 3.843 (Brünger, 1992). In the first stage, structures were calculated using sub-distance geometry embedding followed by simulated annealing and a refinement step. The standard XPLOR protocol in *dg_sub_embed.inp* and *refine.inp* was used for the first and last steps. However, in the second step the *dgsa.inp* protocol was modified to include refinement using the measured values of the $^3J_{H^NH^\alpha}$ coupling constants (Kuszewski *et al.*, 1995; Garrett *et al.*, 1994). The simulated annealing step (*dgsa.inp*) starts at 2500 K with 3500

high temperature and 7500 cooling-steps. The refinement step, which is also dynamical simulated annealing starts at 3000 K with 18,000 cooling-steps. The force constants for the calculation of NOE and dihedral energies in both protocols were 50 and 400 kcal mol^{-1}, respectively. Thirty structures were selected on the criteria that no NOE distance be outside the distance bounds by ±0.5 Å and that dihedral angle restraint violations be $\leqslant 5^\circ$. The programs AQUA and PROCHECK-NMR (Laskowski *et al.*, 1996) were used to check the quality of the computed structures.

Time resolved fluorescence

The time resolved anisotropy decay of the Trp fluorescence was measured using time-correlated single photon counting (O'Connor & Phillips, 1984). Protein samples were excited at 300 nm using the frequency-doubled output of a cavity-dumped, synchronously-pumped Coherent 700 rhodamine 6G dye laser (Coherent, USA) which was itself pumped by the frequency-doubled output of a Coherent Antares YAG laser. The emission was isolated using an interference filter (351 nm; 10 nm bandpass) and detected with a Hamamatsu R2809 microchannel plate photo-multiplier tube (Hamamatsu, Japan). The full width at half maximum of the instrument response function obtained by collecting scattered light from a suspension of non-dairy creamer was 50 ps. Data (2 k channels) were acquired using a Nucleus PCA-II data acquisition card (Oxford Instruments, USA). The parallel ($I_\parallel$) and perpendicular ($I_\perp$) components of the emitted fluorescence were obtained by alternately integrating the respective data sets for 30 seconds until the peak count in the parallel channel was approximately 2×10^4. The decay of the fluorescence anisotropy of Trp102 is given by (Szabo, 1984):

$$r(t) = \frac{I_\parallel(t) - gI_\perp(t)}{I_\parallel(t) + 2gI_\perp(t)} = \sum_{i=1}^{n} \beta_i \exp^{-t/\phi_i} + r_\infty \qquad (6)$$

where $I_\parallel$ and $I_\perp$ are the parallel and polarized components of the intensity decay, g is an optical correction factor and r_∞ is the anisotropy at infinite time. The pre-exponential factors, β_i, and the rotational correlation times, ϕ_i, are functions of the rates of rotation about the molecular axes and the orientation of the absorption and emission dipoles relative to these axes (Belford *et al.*, 1972; Chuang & Eisenthal, 1972; Ehrenberg & Rigler, 1972). Data analysis was performed using the program ANISO (Z. Bajzer *et al.*, unpublished) employing cubic discretization of the instrument response function.

Minimum perturbation mapping

Minimum perturbation maps (Shih *et al.*, 1985; Haydock, 1993) were calculated to determine the possible rotational isomers of the indole side-chain of Trp in F102W parvalbumin and azurin. The structures used to obtain minimum perturbation maps for Trp102 were generated from the coordinates of the average NMR solution structure of F102W determined in this work and those of the two-cadmium X-ray crystal structure of wild-type carp parvalbumin (Swain *et al.*, 1989). For the wild-type protein, the side-chain of Trp102 was built from the topology and parameter internal coordinates. Residues 39, 46, 47, 50, 66, 97, 98, 100, 101, 103, 104 and 105, all of which are within a 5 Å radius of Trp102, were allowed to adjust their conformation to achieve energy minimization during the simulations. The map for azurin was obtained using the X-ray crystal structure of azurin (Nar *et al.*, 1991) and allowing residues 7, 15, 20,31, 33, 46, 47, 49, 50, 82, 83, 84, 85, 95, 97 to adjust their conformation to acheive energy minimization. All non-polar hydrogen atoms were treated as extended heavy atoms and the dielectric constant was made equal to the distance in angstroms between interacting atoms to approximate solvent screening effects (Sharp, 1993). The charge on ionized side-chains was reduced by 80% and non-bonded interactions were switched off over the range 7-11 Å. Calculations were performed on a four-processor R10000 SGI Challenge computer using executable code derived from CHARMM (Brooks *et al.*, 1983) version 23 with topology and parameter files taken from CHARMM version 22.

Minimum perturbation mappings were computed on a 5° grid of Trp102 $\chi_1 \times \chi_2$ torsion space (Haydock, 1993). During minimization, χ_1 and χ_2 were constrained with a harmonic constraint energy constant of 400 kcal mol^{-1} rad^2. At each of the 72×72 grid points, the energy of the free atoms was minimized using 40 steps of the steepest descent method followed by 240 steps with the Powell (1977) method. SHAKE (van Gunsteren & Karplus, 1980) was applied to all bonds involving hydrogen and the system minimized for an additional 40 steps by the Powell method. Grid points for which the final minimized energy exceeded 50 kcal mol^{-1} were considered outliers and the map was interpolated at these points using bivariate interpolation (Akima, 1978). The order parameter for the fluorescence transition dipole was calculated from the miminum perturbation map of F102W as described previously (Haydock, 1993).

Acknowledgements

We thank Dr Christopher Haydock for many helpful discussions and for calculating the ^1L_a and ^1L_b fluorescence order parameters from the minimum perturbation data. We also thank Dr Art Palmer III of Columbia University for making the MODELFREE program available. This work was supported by NIH grants GM34847 to F.G.P. and AR37701 to J.D.P.

References

Abragam, A. (1961). *Principles of Nuclear Magnetism*, Clarendon Press, Oxford.

Akima, H. (1978). A method of bivariate interpolation and smooth surface fitting for irregularly distributed data points. *ACM Trans. Math. Software*, **4**, 148-159.

Akke, M., Skelton, N. J., Kördel, J., Palmer, A. J. & Chazin, W. J. (1993). Effects of ion binding on the backbone dynamics of calbindin D_{9k} determined by ^{15}N NMR relaxation. *Biochemistry*, **32**, 9832-9844.

Alattia, T., Padilla, A. & Cavé, A. (1996). Assignment of ^{13}C resonances and analysis of relaxation properties and internal dynamics of pike parvalbumin by ^{13}C-NMR at natural abundance. *Eur. J. Biochem.* **237**, 561-574.

Alcala, J. R., Gratton, E. & Prendergast, F. G. (1987). Interpretation of fluorescence decays in proteins using continuous distributions. *Biophys. J.* **65**, 2313-2323.

Bajzer, Ž. & Prendergast, F. G. (1993). A model for multiexponential tryptophan fluorescence intensity decay in proteins. *Biophys. J.* **65**, 2313-2323.

Baldellon, C., Alattia, J.-R., Strub, M.-P., Pauls, T., Berchtold, M. W., Cavé, A. & Padilla, A. (1998). ^{15}N-NMR relaxation studies of calcium-loaded parvalbumin show tight dynamics compared to those of other EF-hand proteins. *Biochemistry,* **37**, 9964-9975.

Barbato, G., Ikura, M., Kay, L. E., Pastor, R. W. & Bax, A. (1992). Backbone dynamics of calmodulin studied by ^{15}N relaxation using inverse detected two-dimensional nmr spectroscopy: the central helix is flexible. *Biochemistry,* **31**, 5269-5278.

Beechem, J. M. & Brand, L. (1985). Time-resolved fluorescence of proteins. *Annu. Rev. Biochem.* **53**, 43-71.

Belford, G. G., Belford, R. L. & Weber, G. (1972). Dynamics of fluorescence polarization in macromolecules. *Proc. Natl Acad. Sci. USA,* **69**, 1392-1393.

Brewer, J. M., Wunderlich, J. K., Kim, D.-H., Cass, M. Y., Beach, G. G. & Ragland, W. L. (1989). Avian thymic hormone (ATH) is a parvalbumin. *Biochem. Biophys. Res. Commun.* **160**, 1155-1161.

Brooks, B. R., Bruccoleri, R. E., Olafson, B. D., States, D. J., Swaminathan, S. & Karplus, M. (1983). Charmm: a program for macromolecular energy minimization, and dynamics calculations. *J. Comput. Chem.* **4**, 187-217.

Brünger, A. T. (1992). *X-PLOR 3.1 Manual*, Yale University Press, New Haven, CT.

Callis, P. R. (1997). ^1L_a and ^1L_b transitions of tryptophan: applications of theory and experimental observations to fluorescence of proteins. *Methods Enzymol.* **278**, 113-150.

Cates, S. M., Berry, M. B., Ho, E. L., Li, Q., Potter, J. D. & Phillips, G. N. (1999). Metal ion affinity and specificity in EF-Hand proteins: coordination geometry and domain plasticity in parvalbumin. *Structure,* **In the press**.

Catterall, T. & Duddell, J. (1983). *Time-Resolved Fluorescence Spectroscopy*, vol. 173, Plenum, NY.

Chuang, T. J. & Eisenthal, K. B. (1972). Theory of fluorescence depolarization by anisotropic rotational diffusion. *J. Chem. Phys.* **57**, 5094-5097.

Clore, G. M., Bax, A., Driscoll, P. C., Wingfield, P. T. & Gronenborn, A. M. (1990). Assignment of the side-chain ^{1}H and ^{13}C resonances of interleukin-1β using double- and triple-resonance heteronuclear three-dimensional NMR spectroscopy. *Biochemistry,* **29**, 8172-8184.

Coffee, C. J. & Bradshaw, R. A. (1973). Carp muscle calcium-binding protein. I. Characterization of the tryptic peptides and the complete amino acid sequence of component B. *J. Biol. Chem.* **248**, 3305-3312.

Corsun, D. C., Williams, T. C. & Sykes, B.-D. (1983). Calcium binding proteins: optical stopped-flow and protein nuclear magnetic resonance studies of the binding of the lanthamide series of metal ions to parvalbumin. *Biochemistry,* **22**, 5882-5889.

Eftink, M. R. & Wasylewski, Z. (1989). Fluorescence lifetime and solute quenching studies with the single tryptophan containing protein parvalbumin from codfish. *Biochemistry,* **28**, 382-391.

Ehrenberg, M. & Rigler, R. (1972). Polarized fluorescence and rotational Brownian rotation. *Chem. Phys. Letters,* **14**, 539-544.

Fushman, D., Tjandra, N. & Cowburn, D. (1998). Direct measurement of ^{15}N chemical shift anisotropy in solution. *JACS,* **120**, 10947-10952.

Gagné, S. M., Tsuda, S., Spyracopoulos, L., Kay, L. E. & Sykes, B. D. (1998). Backbone and methyl dynamics of the regulatory domain of troponin C: anisotropic rotational diffusion and contribution of conformational entropy to calcium affinity. *J. Mol. Biol.* **278**, 667-686.

Garrett, D. S., Kuszewski, J., Hancock, T. J., Lodi, P. J., Vuister, G. W., Gronenborn, A. M. & Clore, G. M. (1994). The impact of direct refinement against three-bond HN-C$^\alpha$H coupling constants on protein structure determination by NMR. *J. Magn. Reson.* **104**, 99-103.

Gauduchon, P. & Wahl, P. (1978). Pulsefluorimetry of tyrosyl peptides. *Biophys. Chem.* **8**, 87-104.

Gerstein, M., Tsai, J. & Levitt, M. (1995). The volume of atoms on the protein surface: Calculated from simulation, using Voronoi polyhedra. *J. Mol. Biol.* **249**, 955-966.

Grzesiek, S. & Bax, A. (1992). Improved 3D tripple-resonance NMR techniques applied to a 31 kda protein. *J. Magn. Reson.* **96**, 432-440.

Hansen, J. E., Longworth, J. W. & Fleming, G. R. (1990). Photophysics of metalloazurins. *Biochemistry,* **29**, 7329-7338.

Harpaz, Y., Gerstein, M. & Chothia, C. (1994). Volume changes on protein folding. *Structure,* **2**, 641-649.

Haydock, C. (1993). Protein side chain rotational isomerization: a minimum perturbation mapping study. *J. Chem. Phys.* **98**, 8199-8214.

Hu, W., Lazo, N. D. & Cross, T. A. (1995). Tryptophan dynamics and structural refinement in a lipid bilayer environment: solid state NMR of the gramicidin channel. *Biochemistry,* **34**, 14138-14146.

Hutnik, C. M. & Szabo, A. G. (1989). Confirmation that multiexponential fluorescence decay behavior of holoazurin originates from conformational heterogeneity. *Biochemistry,* **28**, 3923-3934.

Hutnik, C. M., MacManus, J. P., Banville, D. & Szabo, A. G. (1990a). Comparison of metal ion-induced conformational changes in parvalbumin and oncomodulin as probed by the intrinsic fluorescence of tryptophan 102. *J. Biol. Chem.* **265**, 11456-11464.

Hutnik, C. M. L., MacManus, J. P. & Szabo, A. G. (1990b). A calcium-specific conformational response of parvalbumin. *Biochemistry,* **29**, 7318-7328.

Ikura, M., Kay, L. E., Tschudin, R. & Bax, A. (1990). Three dimensional NOESY-HMQC spectroscopy of a ^{13}C-labelled protein. *J. Magn. Reson.* **86**, 204-209.

James, D. R., Liu, Y., De Mayo, P. & Ware, W. R. (1985). Distributions of fluorescence lifetimes: consequences for the photophysics of molecules adsorbed on surfaces. *Chem. Phys. Letters,* **120**, 460-465.

Jeener, J., Meier, B. H., Bachmann, P. & Ernst, R. R. (1979). Investigation of exchange processes by two-dimensional NMR spectroscopy. *J. Chem. Phys.* **71**, 4546-4553.

Joassin, L. & Gerday, C. (1977). The amino acid sequence of the major parvalbumin of the whiting *Gadus merlangus*. *Comp. Biochem. Physiol.* **57B**, 159-161.

Kawasaki, H. & Kretsinger, R. (1994). Calcium binding proteins 1: EF-hands. *Protein Profile,* **1**, 343-349.

Kay, L. E. & Bax, A. (1990). New methods for the measurement of NH-C$_\alpha$H coupling constants in ^{15}N-labelled proteins. *J. Magn. Reson.* **86**, 110-126.

Kay, L. E., Marion, D. & Bax, A. (1989a). Practical aspects of 3D heteronuclear NMR of proteins. *J. Magn. Reson.* **84**, 72-84.

Kay, L. E., Torchia, D. A. & Bax, A. (1989b). Backbone dynamics of proteins as studied by ^{15}N inverse detected heteronuclear NMR spectroscopy: application to staphylococcal nuclease. *Biochemistry,* **28**, 8972-8979.

Kay, L. E., Ikura, M., Tschudin, R. & Bax, A. (1990). Three-dimensional triple-resonance NMR spectroscopy of isotopically enriched proteins. *J. Magn. Reson.* **89**, 496-514.

Kemple, M. D., Yuan, P., Nollet, K. E., Fuchs, J. A., Silva, N. & Prendergast, F. G. (1994). ^{13}C NMR and fluorescence analysis of tryptophan dynamics in wild-type and two single-trp variants of *Escherichia coli* thioredoxin. *Biophys. J.* **66**, 2111-2126.

Kemple, M. D., Buckley, P., Yuan, P. & Prendergast, F. G. (1997). Main chain and side chain dynamics of peptides in liquid solution from ^{13}C NMR: melittin as a model peptide. *Biochemistry,* **36**, 1678-1688.

Kinosita, K., Kawato, S. & Ikegami, A. (1977). A theory of fluorescence polarization decay in membranes. *Biophys. J.* **20**, 289-305.

Kraulis, P. J. (1991). Molscript: a program to produce both detailed and schematic plots of protein structures. *J. Appl. Crystallog.* **24**, 946-950.

Kretsinger, R. H. & Nockolds, C. E. (1973). Carp muscle calcium-binding protein. II. Structure determination and general description. *J. Biol. Chem.* **248**, 3313-3326.

Kretsinger, R. H., Dangelat, D. & Bryan, R. F. (1971). Crystal data for low molecular weight albumins of carp. *J. Mol. Biol.* **59**, 213-214.

Kuszewski, J., Gronenborn, A. G. & Clore, G. M. (1995). The impact of direct refinement against proton chemical shifts on protein structure determination by NMR. *J. Magn. Reson.* **107**, 293-297.

Laskowski, R. A., Rullmann, J. A. C., MacArthur, M. W., Kaptein, R. & Thornton, J. M. (1996). Aqua and Procheck-NMR: programs for checking the quality of protein structures solved by NMR. *J. Biomol. NMR,* **8**, 477-486.

Lipari, G. & Szabo, A. (1982a). Model-free approach to the interpretation of nuclear magnetic resonance relaxation in macromolecules. 1. Theory and range of validity. *JACS,* **104**, 4546-4559.

Lipari, G. & Szabo, A. (1982b). Model-free approach to the interpretation of nuclear magnetic resonance relaxation in macromolecules. 2. Analysis of experimental results. *JACS,* **104**, 4559-4570.

Macura, S. & Ernst, R. R. (1980). Elucidation of cross relaxation in liquids by two-dimensional NMR spectroscopy. *Mol. Phys.* **41**, 95-117.

Mandel, A. M., Akke, M. & Palmer, A. G., III (1995). Backbone dynamics of *Escherichia coli* ribonuclease HI: correlations with structure and function in an active enzyme. *J. Mol. Biol.* **246**, 144-163.

Marion, D. E. K. L., Sparks, S. E., Torchia, D. A. & Bax, A. (1989). Three-dimensional heteronuclear NMR of ^{15}N labelled proteins. *J. Am. Chem. Soc.* **111**, 1515-1517.

Moeschler, H. J., Schaer, J. J. & Cox, J. A. (1980). A thermodynamic analysis of the binding of calcium and magnesium ions to parvalbumin. *J. Eur. Biochem.* **111**, 73-78.

Moews, P. C. & Kretsinger, R. H. (1975). Terbium replacement of calcium in carp muscle calcium-binding parvalbumin: an X-ray crystallographic study. *J. Mol. Biol.* **91**, 229-232.

Nar, H., Messerschmidt, A., Huber, R., van de Kamp, M. & Canters, G. W. (1991). Crystal structure analysis of oxidized *Pseudomonas aeruginosa* azurin at pH 5.5 and pH 9.0. a pH-induced conformational transition involves a peptide bond flip. *J. Mol. Boil.* **221**, 765-772.

O'Connor, D. V. & Phillips, D. (1984). *Time-correlated Single Photon Counting*, Academic Press, NY.

Palmer, A. G., Hochstrasser, R. A., Millar, D. P., Rance, M. & Wright, P. E. (1993). Characterization of amino acid side chain dynamics in a zinc-finger peptide using ^{13}C NMR spectroscopy and time-resolved fluorescence spectroscopy. *J. Am. Chem. Soc.* **115**, 6333-6345.

Pardi, A., Billeter, M. & Wüthrich, K. (1984). Calibration of the angular dependence of the amide proton-C^{α} proton coupling constants, $^{3}J_{HN\alpha}$, in a globular protein. Use of $^{3}J_{HN\alpha}$ for identification of helical secondary structure. *J. Mol. Biol.* **180**, 741-751.

Pauls, T. L. & Berchthold, M. W. (1993). Efficient complementary DNA amplification and expression using polymerase chain reaction technology. *Methods Enzymol.* **217**, 102-122.

Petrich, J. W., Chang, M. C., McDonald, D. B. & Fleming, G. R. (1983). On the origin of nonexponential fluorescence decay in tryptophan and its derivatives. *J. Am. Chem. Soc.* **105**, 3824-3832.

Powell, M. J. D. (1977). Restart procedures for the conjugate gradient method. *Math. Program.* **12**, 241-254.

Ross, J. B. A., Wyssbrod, H. R., Porter, R. A., Schwartz, G. P., Michaels, C. A. & Laws, W. R. (1992). Correlation of tryptophan fluorescence intensity decay parameters with ^{1}H NMR-determined rotamer conformations: [Tryptophan^{2}]Oxytocin. *Biochemistry,* **31**, 1585-1594.

Sambrook, J., Fritsh, E. E. & Maniatas, T. (1989). *Molecular Cloning: A Laboratory Manual*, chapt. 5, pp. 5.44-5.48, Cold Spring Harbor Laboratory Press, Cold Spring Harbor, NY.

Sharp, K. A. (1993). Inclusion of solvent effects in molecular mechanics force fields. In *Computer Simulation of Biomolecular Systems. Theoretical and Experimental Applications* (van Gunsteren, W. F., Weiner, P. K. & Wilkinson, A. J., eds), pp. 147-160, ESCOM, Leiden.

Shih, H. H., Brady, J. & Karplus, M. (1985). Structure of proteins with single-site mutations: aminimum perturbation approach. *Proc. Natl Acad. Sci. USA,* **82**, 1697-1700.

Swain, A. L., Kretsinger, R. L. & Elmer, L. A. (1989). Restrained least squares refinement of native (calcium) and cadmium-substituted carp parvalbumin using X-ray crystallographic data at 1.6 Å resolution. *J. Biol. Chem.* **264**, 16620-16628.

Szabo, A. (1984). Theory of fluorescence depolarization in macromolecules and membranes. *J. Chem. Phys.* **81**, 150-167.

Szabo, A. G. & Rayner, D. M. (1980). Fluorescence decay of tryptophan conformers in aqueous solution. *JACS,* **102**, 554-563.

Turoverov, K. K., Kuznetsova, I. M. & Zaitsev, V. N. (1985). The environment of the tryptophan residue in *Pseudomonas aeruginosa* azurin and its fluorescence properties. *Biophys. Chem.* **23**, 79-89.

van Gilst, M., Tang, C., Roth, A. & Hudson, B. (1994). Quenching interactions and nonexponential decay: tryptophan 138 of bacteriophage {T}4 lysozyme. *J. Fluoresc.* **4**, 203-207.

van Gunsteren, W. F. & Karplus, M. (1980). A method for constrained energy minimization of macromolecules. *J. Comput. Chem.* **1**, 266-274.

Vuister, G. W. & Bax, A. (1993). Quantitative J correlation: a new approach for measuring three-bond $J(H^{N}H^{\alpha})$ coupling constants in ^{15}N-enriched proteins. *J. Am. Chem. Soc.* **115**, 7772-7777.

Yuan, P., Fisher, P. J., Prendergast, F. G. & Kemple, M. D. (1996). Structure and dynamics of melittin in lysomyristoyl phosphatidylcholine micelles determined by nuclear magnetic resonance. *Biophys. J.* **70**, 2223-2238.

Zhu, G. & Bax, A. (1992). Improved linear prediction of damped NMR signals using modified ''forward-backward'' linear prediction. *J. Magn. Reson.* **100**, 202-207.

Zolnai, Z., Juranić, N., Markley, J. L. & Macura, S. (1995). Magnetization exchange network editing: mathematical principles and experimental demonstration. *Chem. Phys.* **200**, 161-179.

Zolnai, Z., Juranić, N., Markley, J. L. & Macura, S. (1996). Zooming, a practical strategy for improving the quality of multi-dimensional NMR spectra. *J. Magn. Reson. ser. A*, **119**, 53-64.

Edited by P. E. Wright

(Received 21 October 1999; received in revised form 19 January 2000; accepted 20 January 2000)

http://www.academicpress.com/jmb

Supplementary material comprising a Table of backbone and side-chain assignments is available from JMB Online